Turk J Phys
29 (2005) , 85 – 90.

Microstructure Characterization of $ZnFe_{2-x}M_xO_4$ (M = Bi, Y and x = 0.1, 0.2) Ferrites by the Rietveld Refinement

Mansour AL-HAJ
Physics Department, Mu'tah University, Al-Karak-JORDAN
e-mail: mansour@mutah.edu.jo

Received 06.10.2004

Abstract

The microstructure of the ferrites was analyzed by the Reitveld refinement method. The Bi-containing ferrites revealed a decrease in the lattice parameter as the Bi^{3+} concentration is increased, due to the distortion of the ferrite lattice. There was a minor distortion in the $ZnFe_{1.9}Y_{0.1}O_4$ ferrite lattice. A minor yttrium oxide phase coexisted with the $ZnFe_{1.8}Y_{0.2}O_4$ spinel phase.

Key Words: Ferrites; X-ray diffraction; lattice parameter; paramagnetic; magnetization.

PACS: 75.60.Ej, 75.50.Gg

1. Introduction

Ferrites are an important class of magnetic materials due to their technological applications [1, 2]. The general chemical formula of a ferrite is AFe_2O_4, where A is a divalent element. The cubic ferrites have the spinel crystal structure of the type $MgAl_2O_4$. In the normal spinel arrangement the A^{2+} cations occupy only tetrahedral sites, while the Fe^{3+} cations occupy only octahedral sites. In the inverse spinel arrangement the tetrahedral sites are occupied by the Fe^{3+} cations, while the octahedral sites are occupied half by the A^{2+} cations and half by the Fe^{3+} cations.

$ZnFe_2O_4$ is a normal spinel ferrite at room temperature and has been the subject of extensive research spanning decades. The formation of normal and inverse spinel structures was observed in nanocrystalline $ZnFe_2O_4$ ferrite prepared by mechanical milling and the degree of inversion increased with increasing milling time [3, 4]. It was found that the replacement of the nonmagnetic Y^{3+} cations instead of Fe^{3+} cations in $Zn_{0.5}Ni_{0.5}Y_xFe_{2-x}O_4$ ferrites caused a deformation for the octahedral site after $x = 0.04$ [5].

Magnetic measurements on $Zn_xNi_{1-x}Fe_2O_4$ ferrites [6] showed lower coercivity and higher magnetization values for microwave sintered specimens compared with specimens sintered conventionally. A plot of dielectric constant versus temperature reveal a transition near the Curie temperature for the Zn−Ni−Er ferrites [7], indicating that its behavior may be due to a magnetic transition. The electrical conductivity was found to decrease with increasing Cr content in $Ni_{0.6}Zn_{0.4}Cr_xFe_{2-x}O_4$ ferrites [8], which was explained in terms of the cation valences and distribution. The temperature dependence of initial permeability for Mn-doped Ni−Cu−Zn ferrites showed a decrease in the Curie temperature with increasing Mn content [9], suggesting the incorporation of the Mn ions into the ferrite lattice. It was reported that the preferences of Zn^{2+}

to tetrahedral sites and the replacement of Cr^{3+} ions at the expense of the Fe^{3+} ions on the octahedral sites affect directly the behavior of the magnetic susceptibility of $Zn_{1-x}Cu_xCr_{0.8}Fe_{1.2}O_4$ ferrites [10]. The mechanically milled $Zn_{0.8}Co_{0.2}Fe_2O_4$ spinel showed an enhancement in both magnetization and ordering temperature compared with the bulk sample [11]. The replacement of Fe^{3+} by La^{3+} on octahedral sites and the presence of Co^{2+} and Zn^{2+} ions on the tetrahedral sites were found to play a significant role in the electrical and magnetic properties of Co−Zn−La ferrites [12].

The aim of our work is to investigate the microstructure of $ZnM_xFe_{2-x}O_4$ ferrites (M = Bi, Y and x = 0.1, 0.2) by the Rietveld refinement method. The main advantages of this analysis method are that we can obtain accurate values of the structural parameters and identify the type of cations occupying the tetrahedral and octahedral sites and their probability of occupation.

2. Experimental Procedure

The ferrite powders were prepared by the usual ceramic method. Analytical grade oxides (ZnO, Fe_2O_3, Bi_2O_3, Y_2O_3) were mixed, ground and sintered at 1100 °C in a Carbolite furnace for 10 h. Each sample was then cooled slowly to room temperature, ground and sintered again at 1100 °C for 10 h. The X-ray diffraction (XRD) patterns were taken using a Seifert 3003 TT diffractometer operating at 40 kV and 40 mA. The experimental setup is: Cu source / Ni filter / 3 mm slit / primary collimator / 2 mm slit / sample / 4 mm slit / secondary collimator / 0.1 mm slit / detector, as shown in Figure 1. The angular range is 15−95°, the scan step is 0.01° and the measuring time is 1 s. The diffractometer was calibrated using a standard Si powder. The magnetic measurements were done at room temperature using a 9600 LDJ vibrating sample magnetometer.

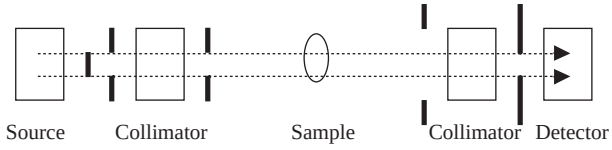

Figure 1. The XRD experimental setup.

3. Method of Analysis

The Rietveld refinement was done using the program AutoQuan [13], an optimization procedure to fit a model of the examined sample to the measured diffraction pattern. A parameter set is used for fitting. The model is refined by minimizing, by a least-squares process, the residual

$$\sum_i w_i(y_i - y_{ic})^2, \tag{1}$$

where $w_i = y_i^{-1}$ is a weight for the i^{th} measuring point, y_i is the measured counts of the i^{th} point and y_{ic} is the calculated counts of the i^{th} point; y_{ic} is the sum of the contributions from all Bragg reflections k out of the phase j being part of the sample:

$$y_{ic} = y_{ib} + \sum_{j,k} S_j P_{jk} m_{jk} L_{jk} T_{jk} |F_{jk}|^2, \tag{2}$$

where y_{ib} is the background of the i^{th} point, S_j is a scale factor, P_{jk} is the profile function, m_{jk} is the multiplicity of the reflection k, L_{jk} is the Lorentz polarization factor, T_{jk} is the isotropic Debye-Waller factor for thermal diffuse scattering spread and F_{jk} is the structure factor.

The background y_{ib} is fitted by a polynomial whose order is determined automatically. The preferred orientation is modeled by the mathematical model of spherical harmonics. The profile function is taken as a convolution of the wavelength distribution, the geometry function and the sample function. A Lorentzian function is taken for the sample function:

$$L = \frac{1}{\pi} \cdot \frac{b}{b^2 + (x - x_0)^2}, \tag{3}$$

where x_0 is the peak position represented by lattice constants and b is the reflection broadening parameter due to crystalline size.

The agreement between the observations and the model is indicated by the goodness of fit:

$$GOF = \frac{\sum\limits_i w_i (y_i - y_{ic})^2}{N - P}, \tag{4}$$

where N and P are the number of profile points and refined parameters, respectively; GOF should approach the ideal value of unity.

4. Results and Discussion

The XRD patterns of the samples $ZnFe_2O_4$, $ZnFe_{1.9}Bi_{0.1}O_4$, $ZnFe_{1.8}Bi_{0.2}O_4$ and $ZnFe_{1.9}Y_{0.1}O_4$ confirmed the single phase spinel structure. For example, the XRD pattern of the sample $ZnFe_{1.8}Bi_{0.2}O_4$ is shown in Figure 2. The structural model is taken as the spinel phase with the space group $Fd\overline{3}m$. The refined parameters such as the lattice and atomic parameters are adjusted until the GOF approaches unity. The results of the analysis are shown in Table. The graphical representation of the measured values, calculated diagram, background (top part of the figure), and difference curve (bottom part of the figure) for $ZnFe_{1.9}Y_{0.1}O_4$ and $ZnFe_{1.8}Y_{0.2}O_4$ are shown in Figure 3 and Figure 4, respectively. It is seen from Table that the GOF values are very close to unity.

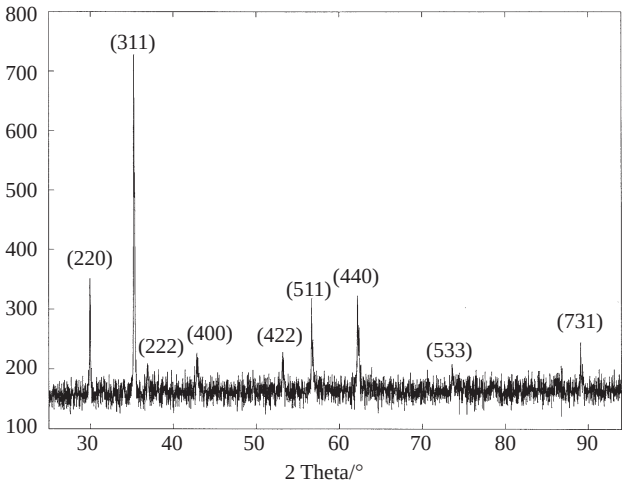

Figure 2. The XRD pattern of $ZnFe_{1.8}Bi_{0.2}O_4$ ferrite.

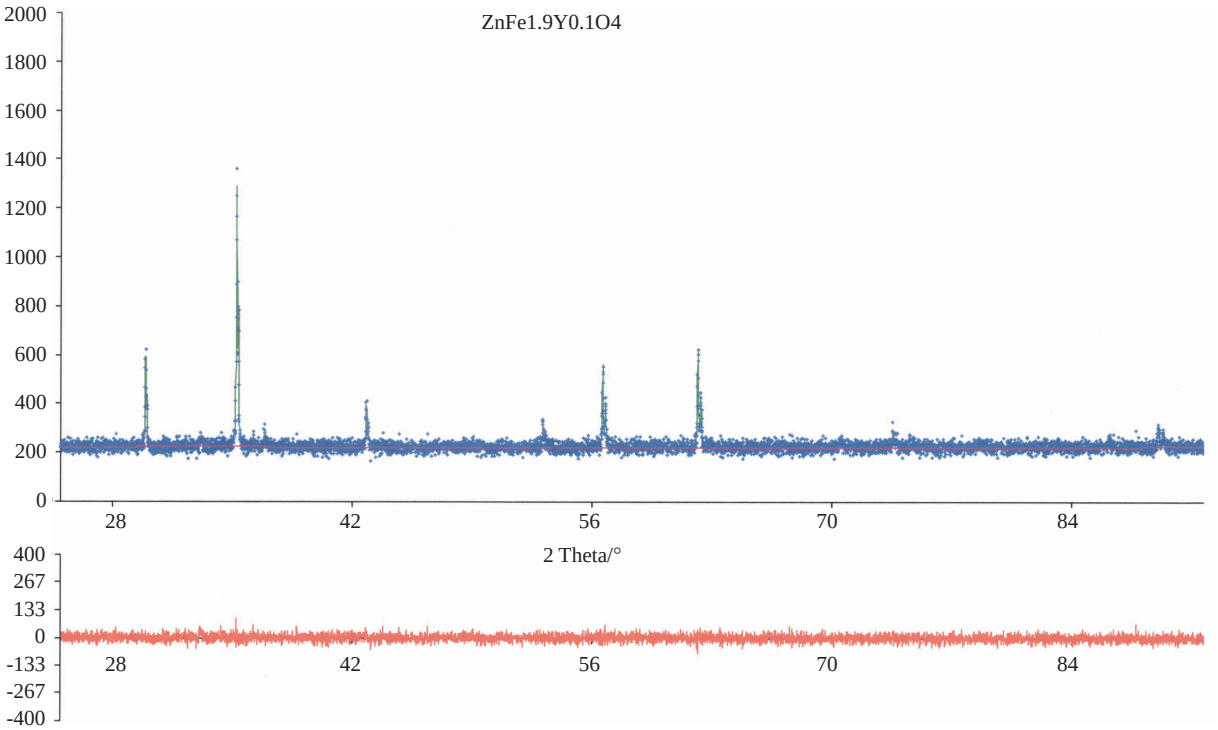

Figure 3. The graphical representation of the Rietveld refinement results for $ZnFe_{1.9}Y_{0.1}O_4$.

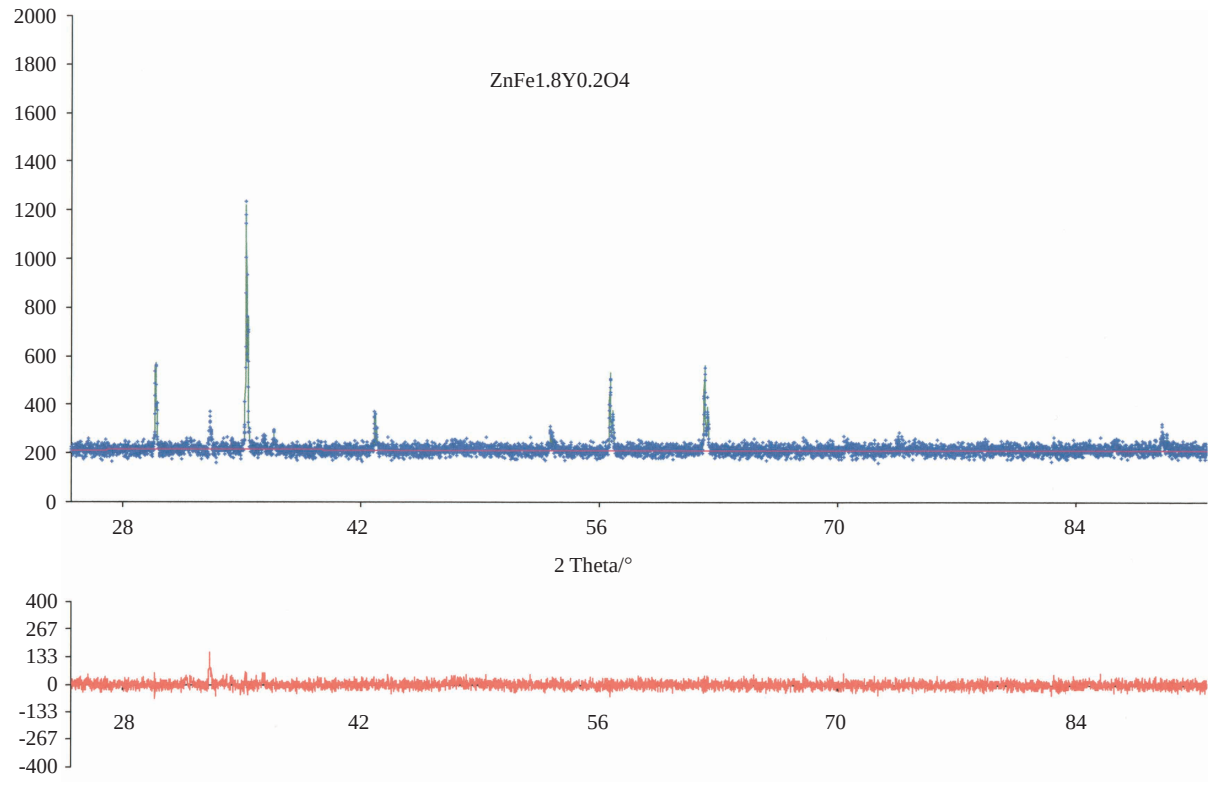

Figure 4. The graphical representation of the Rietveld refinement results for $ZnFe_{1.8}Y_{0.2}O_4$.

Table

Sample	Lattice parameter (Å)	Average grain size (μm)	GOF	Probability of occupation by O^{2-} ions
$ZnFe_2O_4$	8.4412	0.260	1.0045	100%
$ZnFe_{1.9}Bi_{0.1}O_4$	8.4376	0.190	1.0172	84%
$ZnFe_{1.8}Bi_{0.2}O_4$	8.4336	0.140	1.0155	82%
$ZnFe_{1.9}Y_{0.1}O_4$	8.4399	0.267	1.0106	99%
$ZnFe_{1.8}Y_{0.2}O_4$	8.4403	0.263	1.0697	88%

The replacement of a cation by a larger one in ferrites is known to cause an increase in the lattice parameter, as reported for $Ni_{0.3}Mn_xZn_{0.7-x}Fe_2O_4$ ferrites [14], provided that the radius of the substituting cation is not much larger than those of the ferrite cations. The replacement of a cation by a smaller one causes a decrease in the lattice parameter, as reported for $Mg_xAl_{2x}Li_{0.5(1-x)}Fe_{2.5(1-x)}O_4$ ferrites [15]. From Table, we see that the replacement of Fe^{3+} cations (radius = 0.645 Å) by Bi^{3+} cations (radius = 1.03 Å) on the octahedral sites has caused a decrease in the lattice parameter, compared to that of $ZnFe_2O_4$. As the concentration of Bi^{3+} cations is increased, the distortion in the ferrite lattice (vacancies on the O^{2-} sites) increases due to the relatively high radius of Bi^{3+}, compared to that of Fe^{3+}. This is evidenced by the decrease in the probability of occupation by O^{2-} ions. Therefore, the lattice parameter has decreased.

In the case of $ZnFe_{1.9}Y_{0.1}O_4$ ferrite (Figure 3), the Y^{3+} cations (radius = 0.900 Å) have replaced the Fe^{3+} cations on the octahedral sites, but there is a small decrease in the lattice parameter due to the minor distortion in the lattice (the probability of occupation is 99%). As the concentration of Y^{3+} is increased to 0.2, we notice from the XRD pattern (Figure 4) that there is a weak Bragg peak at $2\theta = 33.2°$. The oxide phase Y_2O_3 (ICDD PDF # 44 – 0399) has a strong Bragg peak at $2\theta = 33.2°$. Therefore, a minor Y_2O_3 oxide phase exists besides the major spinel phase at this concentration. The results obtained from the refinement procedure for the $ZnFe_{1.8}Y_{0.2}O_4$ sample are not in contradiction with those for the previous ones since the starting model for refinement was taken as a single spinel phase. This is evidenced by the higher *GOF* value for this sample.

The average grain size for all samples prepared by the conventional method is between 0.1 μm and 1.0 μm. This is a requirement for successful Rietveld refinement, since very small grains (< 0.1 μm), which can be obtained by mechanical milling, will cause profile broadening.

Magnetically, all samples are paramagnetic at room temperature. The results for Y-containing samples are shown in Figure 5. The slope of the line for $ZnFe_{1.8}Y_{0.2}O_4$ is smaller than that for $ZnFe_{1.9}Y_{0.1}O_4$ due

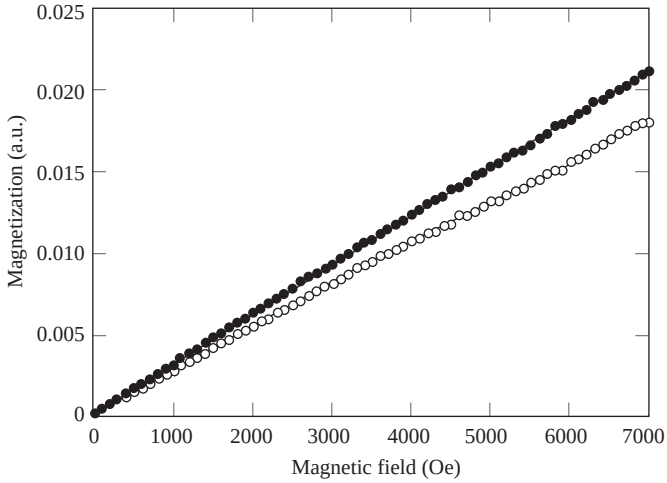

Figure 5. The magnetization curves for $ZnFe_{1.9}Y_{0.1}O_4$ (•) and $ZnFe_{1.8}Y_{0.2}O_4$ (○) samples.

to the presence of the Y_2O_3 oxide. The aim of such magnetic measurements is to make sure that the weak Bragg peak at $2\theta = 33.2^\circ$ is that of an intermetallic phase, not from the scatter of the XRD data. No change in slope was observed for Bi-containing samples.

5. Conclusions

As the concentration of Bi^{3+} is increased in Bi-containing ferrites, the vacancies on the O^{2-} sites are increased due to the large radius of Bi^{3+}, compared to that of Fe^{3+}.

There is a very small distortion in the $ZnFe_{1.9}Y_{0.1}O_4$ ferrite lattice due to the relatively small radius of Y^{3+}, compared to that of Bi^{3+}.

A minor yttrium oxide coexisted with the major $ZnFe_{1.8}Y_{0.2}O_4$ spinel phase.

References

[1] N. Rezlescu, E. Rezlescu, C. Sava, F. Tudorache and P. Popa, *Phys. Stat. Sol.* (a), **201**, (2004), 17.

[2] L. John Berchmans, R. Kalai Selvan and C. Augustin, *Mater. Lett.*, **58**, (2004), 1928.

[3] H. Ehrhardt, S. Campbell and M. Hofmann, *Scripta Mater.*, **48**, (2003), 1141.

[4] S. Bid and S. Pradhan, *Mater. Chem. Phys.*, **82**, (2003), 27.

[5] M. Ahmed, N. Okasha and L. Salah, *J. Magn. Magn. Mater.*, **264**, (2003), 241.

[6] P. Yadoji, R. Peelamedu, D. Agrawal and R. Roy, *Mater. Sci. Eng.*, **B98**, (2003), 269.

[7] K. Kumar, A. Reddy and D. Ravinder, *J. Magn. Magn. Mater.*, **263**, (2003), 121.

[8] A. El-Sayed, *Mater. Chem. Phys.*, **82**, (2003), 583.

[9] Z. Yue, J. Zhou, Z. Gui and L. Li, *J. Magn. Magn. Mater.*, **264**, (2003), 258.

[10] N. Okasha, *Mater. Chem. Phys.*, **84**, (2004), 63.

[11] R. Bhowmik, R. Ranganathan, S. Sarkar, C. Bansal and R. Nagarajan, *Phys. Rev. B* , **68**, (2003), 134433.

[12] M. Ahmed, N. Okasha and M. Gabal, *Mater. Chem. Phys.*, **83**, (2004), 107.

[13] Seifert Analytical X-ray, AutoQuan, version 2.60, 2002.

[14] A. Singh, T. Goel and R. Mendiratta, *Jpn J. Appl. Phys.*, **42**, (2003), 2690.

[15] K. Modi, J. Gajera, M. Chhantbar, K. Saija, G. Baldha and H. Joshi, *Mater. Lett.*, **57**, (2003), 4049.